Microelectronics Reliability 87 (2018) 81–88

Contents lists available at ScienceDirect

Microelectronics Reliability

journal homepage: www.elsevier.com/locate/microrel

A comprehensive solution for electronic packages' reliability assessment with digital image correlation (DIC) method

Yuling Niu*, Jing Wang, Shuai Shao, Huayan Wang, Hohyung Lee, S.B. Park

Opto-Mechanics and Physical Reliability Laboratory, State University of New York at Binghamton, Binghamton, NY 13902, United States

ARTICLE INFO

Keywords:
Digital image correlation
Electronic package
Reliability assessment
Warpage

ABSTRACT

The reliability assessment of electronic packages demands more accurate and efficient method for evaluating heterogeneous packages and their interconnects in various measurement conditions. The digital image correlation (DIC) method has been fully developed in the last decade. With proper improvement, this work demonstrates that DIC method has the ability to fulfill various experimental tasks and obtain the information for interconnect strain analysis, coefficient of thermal expansion (CTE) characterization, in-plane displacement and out-of-plane warpage quantification within one measurement. To some extent, it serves as a comprehensive tool for electronic packages' reliability assessment. Given that the DIC technique is new to the electronic packaging area, this work illustrates the principle of optical non-contact experiment method and presents several improvements to fit for the measurement on electronic packaging area. With these applications, it is foreseeable that the DIC method will play an important role in the reliability assessment of electronic packages.

1. Introduction

Devices that enhance the performance while miniaturizing the dimension is an obstacle for the development of electronic packages because it challenges reliability [1]. In order to evaluate the reliability of electronic packages, conventional tools, such as Thermo-Mechanical Analyzer (TMA), and Moiré techniques, were employed to assist the property characterization and warpage quantification [2, 3]. With the rapid development of electronic packages, more sophisticated structure and diminutive interconnect arrived. However, experiment instruments were not implemented correspondingly; they merely quantify the displacement in one direction for each test [4]. The out-of-plane deformation is a potential error source because these tools assume exclusively the occurrence of in-plane deformation [5, 6]. The fringe interference tools demand a glass grating on sample surface to generate fringes [7]. These methods also request the specimen preparation in a certain size. The low measurement efficiency and stringent requirements of specimen preparation hampers the reliability evaluation progress. High magnification microscope observes the interconnect failure, or the formation of intermetallic layer, which is confined to displaying the visible phenomenon [8]. The potential risks, such as the strain concentration or expansion mismatch, cannot be quantified. The exploration of experiment methods fails to catch up with the relatively dilatory development of electronic packages.

The digital image correlation (DIC) method refers to an optical and non-contact measurement technique, which includes the steps of image acquisition, storage, and correlation since the 1980s [9–11]. It generates the full-field deformation, motion, and profile in all the directions [12]. Benefiting from the enhancement of pixel amount, DIC method evolved to be a technique for the in-situ mechanics test with high sensitivity [13]. Numerous works demonstrate the effectiveness and accuracy of DIC technique in solid mechanics, such as tensile test [14, 15]. Park et al. [16, 17] introduced the DIC method to the microelectronics reliability assessment and improved the experiment system to accommodate the demands for measuring electronics under thermal and mechanical loading. Meanwhile, it is capable of monitoring multiple plateaus at real time [18]. Since the DIC method was devised, many efforts have been made to compare DIC and Moiré method. The deformation of BGA was measured with both methods and the results were consistent [7]. The JEDEC standard for warpage measurement method [19] also includes both 3-D DIC and Shadow Moiré as the recommended test methods, which means the two methods have been demonstrated as reliable tools to assist the reliability assessment of electronic packages.

Although many labs are equipped with the DIC system, they are confined to using the 3-D DIC to describe the warpage of electronic packages [20, 21]. Actually, when the DIC system is established and calibrated, the 2-D function is capable of characterizing the strain concentrations on the interconnects [22] or the intermetallic material property [23]. If the focal lens is substituted for a high magnification

* Corresponding author.
E-mail address: yniu1@binghamton.edu (Y. Niu).

https://doi.org/10.1016/j.microrel.2018.06.006
Received 8 January 2018; Received in revised form 25 March 2018; Accepted 7 June 2018
Available online 15 June 2018

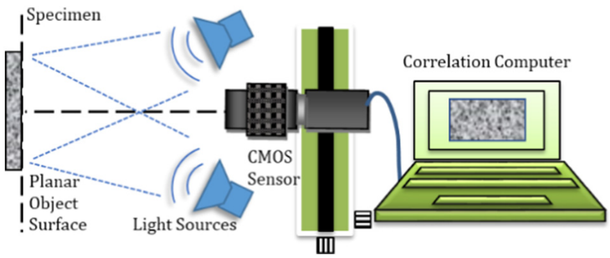

Fig. 1. Schematic of 2-D DIC experiment system.

lens or Scanning Electron Microscope (SEM) [24], the local strain of the interconnects displays the chip package interaction [25]. The 3-D DIC generates the full-field in-plane strain efficiently, while the out-of-plane deformation are calculated and even included in the in-plane strain analysis. Furthermore, the high-speed camera DIC system can capture the instantaneous shock of the devices [26, 27]. Through this work, some innovative applications and developments of the DIC technique are introduced. A consummate inspection of electronic packages can be conducted macroscopically and microscopically with the DIC system. This work summarizes the functions of the DIC method to instruct the users how to employ this technique thoroughly and update the experiment method from the conventional ways. Some novel ideas based on the demands of electronic packages have been proposed, built, and applied. It is expected that the complex test conditions and electronic packages' structures can be resolved with the DIC technique.

2. Methodologies of 2-D DIC

The in-plane 2-D DIC (Fig. 1) derives from the concept that camera traces the feature movement on the sample surface. The camera sensor focuses on the planar object surface to record the images of the specimen under different loads. The specimen was painted or sprayed with black and white patterns as the features to give each pixel a grey value that ranges between 0 (black) and 255 (white). The light sources are important to illuminate the white and black features on the sample surface. In addition, the basic calculation unit is subset, which consists of several pixels (the green rectangular in Fig. 2). By grouping many pixels into one subset, it is capable of correlating and recognizing the shape and displacement of every subset. The shear deformation can be justified through the subset shape comparison. 2-D DIC achieves a 0.02 pixel measurement accuracy [28].

Fig. 3 interprets the subset in-plane correlation principle. The reference 4 × 4 pixels square subset is the correlation reference when the specimen was not loaded. After the loading was applied, the subset moved to the new position and the shape of the subset was deformed in the dash line. The shape of the subset changes from a square to a parallelogram, which indicates the occurrence of both displacement and distortion. Two intensity points in the subset, A and B, were recognized as a and b in the deformed subset. By mapping the image stages, the correlation system depicts the identical subset before and after load. Based on the continuum mechanics, six parameters (u, v, $\frac{\partial u}{\partial X}$, $\frac{\partial u}{\partial Y}$, $\frac{\partial v}{\partial Y}$, $\frac{\partial v}{\partial X}$) are employed to describe the transformation from the initial subset to a new configuration. Every two parameters define the displacement, expansion or contraction, and rotation. If $A(X, Y)$ and $B(X + \Delta X,\ Y + \Delta Y)$

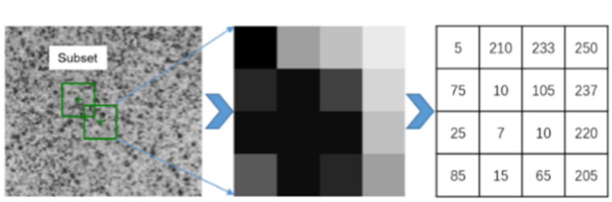

Fig. 2. Example of a 4 × 4 pixels subset assignment and the relevant grey value matrix.

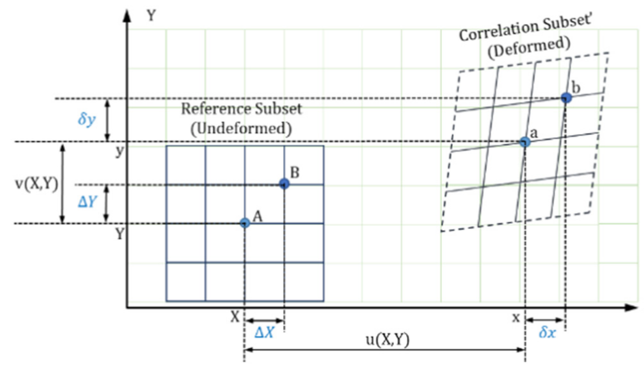

Fig. 3. The schematic of one subset correlation from undeformed status to the loaded status.

are two typical intensity points in reference subset, the relevant points are $a(x,y)$ and $b(x + \delta x, y + \delta y)$ in the deformed subset. The intensity values are expressed as

$$I(A) = I(X, Y) \tag{1}$$

$$I(B) = I(X + \Delta X, Y + \Delta Y) \tag{2}$$

The deformed point a and b can be written based on the parameters of point A and B as follows:

$$a(x, y) = a(X + u, Y + v) \tag{3}$$

$$b(x + \delta x, y + \delta y) = b[X + \Delta X + u(X + \Delta X, Y + \Delta Y), Y + \Delta Y + v(X + \Delta X, Y + \Delta Y)] \tag{4}$$

Then, the intensities for deformed subset are expressed by implementing Eqs. (3) and (4) into the intensity value format [28]:

$$I'(a) = I'(x, y) = I'\ [X + u(X, Y), Y + v(X, Y)] \tag{5}$$

$$I'(b) = I'(x + \delta x, y + \delta y) = I'[X + \Delta X + u(X + \Delta X, Y + \Delta Y), Y + \Delta Y + v(X + \Delta X, Y + \Delta Y)] = I'\left(X + u(X, Y) + \left(1 + \frac{\partial u}{\partial X}\right)\cdot\Delta X + \frac{\partial u}{\partial Y}\cdot\Delta Y, Y + v(X, Y) + \left(1 + \frac{\partial v}{\partial Y}\right)\cdot\Delta Y + \frac{\partial u}{\partial X}\cdot\Delta X\right) \tag{6}$$

With numerous determinations of these six parameters (u, v, $\frac{\partial u}{\partial X}$, $\frac{\partial u}{\partial Y}$, $\frac{\partial v}{\partial Y}$, $\frac{\partial v}{\partial X}$) for all the intensity points, the correlation process is completed, and the deformation information can be determined by adding all the subset deformation together. Meanwhile, the biquadratic spline interpolation was applied to establish a successive intensity allocation in the correlation stages to obtain sub-pixel accuracy when calculating the displacement, which will express the digital pattern intensity in a certain function with a sustained format [28].

3. Reliability studies of electronic packages with 2-D DIC

2-D DIC generates the full-field strain with a broad view ranges as long as the single camera focuses on the sample surface. The robustness makes 2-D DIC an efficient method to cover the small-scale field of view measurement task, like the evaluation of interconnect. When applied to the small-scale packages' reliability assessment, 2-D DIC interprets the potential failures, such as the strain concentration or material interaction, which is not directly visible with microscope.

The interconnects of a flipchip package are scanned with X-ray (*XY* plane) and a symmetric cross-section surface of solder bump (*YZ* plane) is prepared to learn the strain accumulation after temperature changes (Fig. 4). The two bumps at edge column, one in the center of the edge column and the other one at the upper right corner, are selected; they may fail at first. Given that the package dimension is much larger than the bump size, they can be local treated as plane strain condition in *YZ*

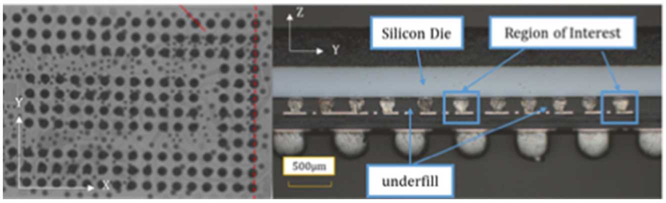

Fig. 4. The X-ray and the cross-section image of flipchip package.

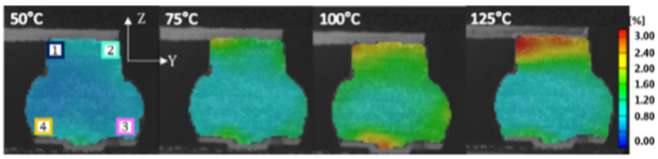

(a)

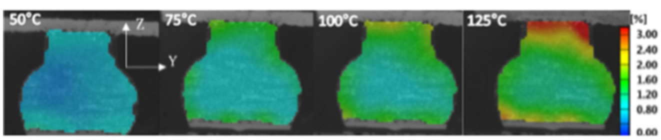

(b)

Fig. 5. The Von Mises strain of the interconnects along edge column, (a) at corner, (b) in the center.

plane. The silicon die, copper pad, and underfill interacted to compress or pull each other because of the CTE mismatch. Fig. 5 shows the Von Mises stress of these two interconnects from room temperature to 125 °C. Room temperature is set as the zero strain reference stage. It explicitly shows the strain concentration at the area close to the copper pad as the loading increases. The bonding from die to solder is stable. The center one deforms less than the corner one from room temperature to 100 °C. At 125 °C, both interconnects show similar strain concentration, but the corner one has shear strain, which makes the strain contour tilt, while the center solder initializes the strain at the board between chip and solder.

The averaged normal (ε_{yy}) and shear (χ_{xy}) strain for each interconnect and the Von Mises strain at the four corners, which are highlighted in Fig. 5(a), are plotted in the diagram (Fig. 6). As the temperature rises, the bump interacts with the die, copper pad, and underfill. The strain accumulation varies at different locations. Compared to the averaged normal and shear strain of the interconnect, the diagram indicates these four corners absorbed most of the energy during the temperature ramp. It explicitly displays the fact that the corner bump endures higher loading than the center one because the corner bump is farthest from the die center and undergoes the maximum strain. Furthermore, the warpage pulls the interconnect between the chip and the substrate, which leads to higher average normal strain on the corner bump.

Besides the cumulative strain of the interconnects, the material interactions can be reported through 2-D DIC with high magnification lens. Currently, the interconnects are miniaturized, which made them easily affected by surrounding materials. Fig. 7 shows an interconnect at the package corner with the underfill around it. The underfill and the solder alloy requires different shutter time, so they are solved separately. At each temperature stage, two images are collected and calculated. The Y direction strain was calculated and analyzed. To understand the bump layer impact on other layers, the ε_{yy} strain difference of two points near the boundary, from point 1 to point 2, are plotted in Fig. 7. It shows that the repeated data points overlapped each other at the same temperature stages along X axis, which proves the stability of the measurement. In the bump and underfill strain contours, the white

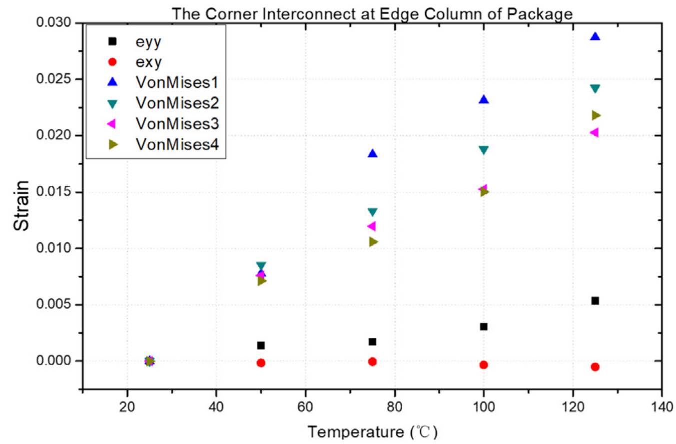

(a)

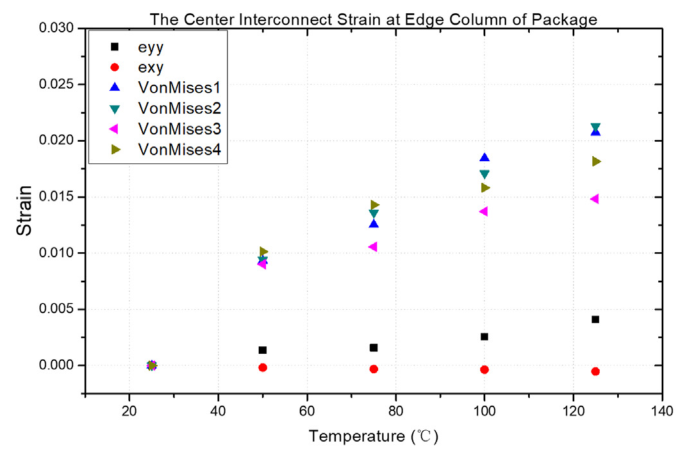

(b)

Fig. 6. The Von Mises strain at four corners of the bump, and the averaged normal strain and shear of the bump (a) at corner of the edge column, (b) in the center of the edge column.

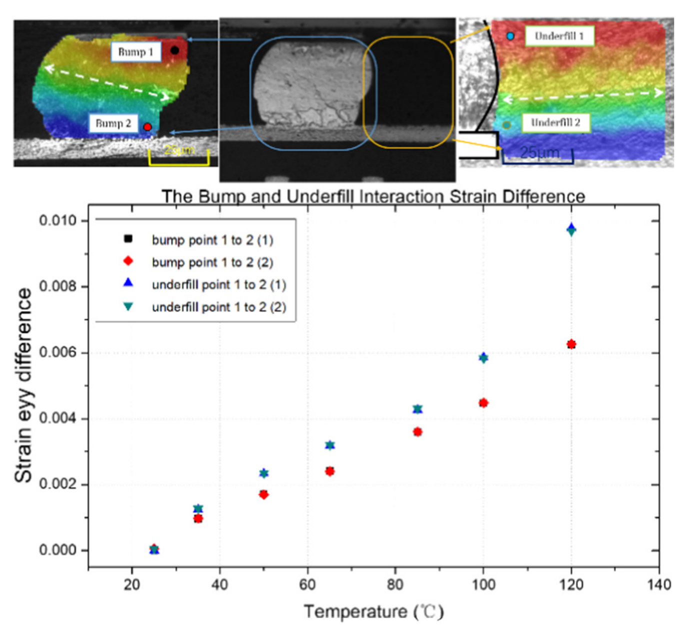

Fig. 7. The relative expansion strain differences of the bump and adjacent underfill at different temperatures.

line in the center is set as the reference line (the transition from green to yellow), and the expansion strain was calculated on the basis of it. Positive and negative strain means the expansion along positive or negative Y axis respectively. At the same temperature, the underfill has a larger relative expansion than the interconnect, which means the polymer stretched the interconnect between copper pad and die. When the temperature approaches underfill glass transient temperature (T_g), beyond 100 °C, the phenomenon is more evident and intense because the CTE of underfill increases after T_g point. It reveals the unnoticeable potential risk in such a small area. These 2-D DIC outputs also serve as simulation reference to calibrate the detailed chip packaging interaction model.

In recent studies, the advanced 2-D DIC devotes itself to measuring the microscopical views. The SEM based DIC technique provides the strain analysis within several micrometers [24]. With this technique, the microscope image could illustrate not only the failure analysis, but also the strain concentration or the component displacement in a small-scale. On one hand, the SEM DIC currently fills the vacancy left by the small field of view for performing the stress analysis on the microbump, the copper pillar, or low dielectric material interaction. However, some challenges still need to be addressed, such as the out-of-plane rigid expansion with the thermal loading, the small patterns generation on different material surfaces, or the tiny disturbance in SEM chamber.

4. Principles of 3-D DIC

3-D DIC utilizes a pair of sensors that are oriented symmetrically to imitate the human perspective and justify both in-plane and out-of-plane deformation (Fig. 8). Experience assists people in estimating the length and the distance of the object. Similarly, calibration helps 3-D DIC to learn the experience course and quantifies the deformation. The 3-D DIC calibration utilizes the calibration panel, which has the standard dots and lines on it. The distances between two dots are standardized and stored in the algorithm. By taking several images of the calibration panel, 11 parameters, related to camera orientation, are determined. There are five intrinsic parameters: focal length f; the center locations C_x and C_y of image plane; the aspect ratio λ; and the radial lens distortion factor k. The six extrinsic parameters include camera rotation matrix, which is expressed with Euler angles (α, β, γ), and the coordinate translation vector (T_x, T_y, T_z). Each angle represents the rotation of each axis respectively. The rotation matrix R, which represents the consecutive spin from the world coordinate to the camera coordinate, is the critical factor to define camera orientation. It follows the Eqs. [28]:

$$\begin{bmatrix} R_{11} & R_{12} & R_{13} \\ R_{21} & R_{22} & R_{23} \\ R_{31} & R_{32} & R_{33} \end{bmatrix} = \begin{bmatrix} \cos\alpha\cos\gamma & -\sin\alpha\cos\gamma & \sin\gamma \\ \sin\alpha\cos\beta + \cos\alpha\sin\beta\sin\gamma & \cos\alpha\cos\beta - \sin\alpha\sin\beta\sin\gamma & -\sin\beta\cos\gamma \\ \sin\alpha\sin\beta - \cos\alpha\cos\beta\sin\gamma & \cos\alpha\sin\beta + \sin\alpha\cos\beta\sin\gamma & -\cos\beta\cos\gamma \end{bmatrix} \quad [7]$$

The rotation matrix [7] and the intrinsic parameters determine the scale that each pixel represents from the actual sample to the digital image. To complete the 3-D profiling, the image is divided into many subsets, and each of them consists of several pixels, as a virtual plane. The features on each subset are consistently recorded by the synchronized cameras at different loadings. In Fig. 8, a square subset in the left image is shown as a parallelogram in the right image because of the camera angle. After correlating the relevant subset from the left and right image, the orientation and position of the virtual plane are defined. A curved surface can be approximated by combining many finite virtual planes together and smoothing them into a continuous surface [29]. When the sample was loaded, the shape and location of the subset (white dash line) was changed compared to the initial status (green line). The changes of all the subsets were recognized and combined to export the total deformation. For the electronic packages test, the environmental chamber imitates the reflow process during the assembly process and guarantees the samples are uniformly heated. With 3-D DIC system, it is feasible to obtain various pieces of information and guide the design, material selection, and manufacturing process.

5. Comprehensive reliability assessments of electronic packages with 3-D DIC

Many researchers regard the 3-D DIC as an alternative warpage measurement method as compared to the conventional ones, e.g., Shadow Moiré. On one hand, Shadow Moiré is convenient when evaluating the warpage of electronic packages, because it has been developed for several decades with simple operation. 3-D DIC requires the intricate calibration and camera adjustment because the new technique has not yet been fully modularized. On the other hand,3-D DIC generates more outputs to pay back for its calibration efforts.

Fig. 9 shows a warpage verification from 3-D DIC to the simulation model, which is an effective way to determine or tune the model. A $60 \times 60\,mm^2$ 2.5-D package is mounted on the PCB, which makes the

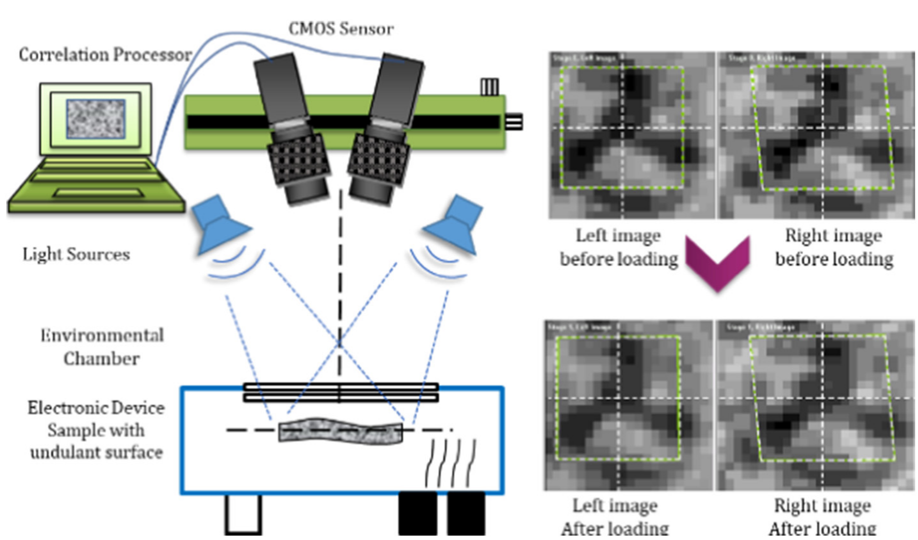

Fig. 8. The schematic of 3-D DIC experiment system and the subset correlation before and after loading.

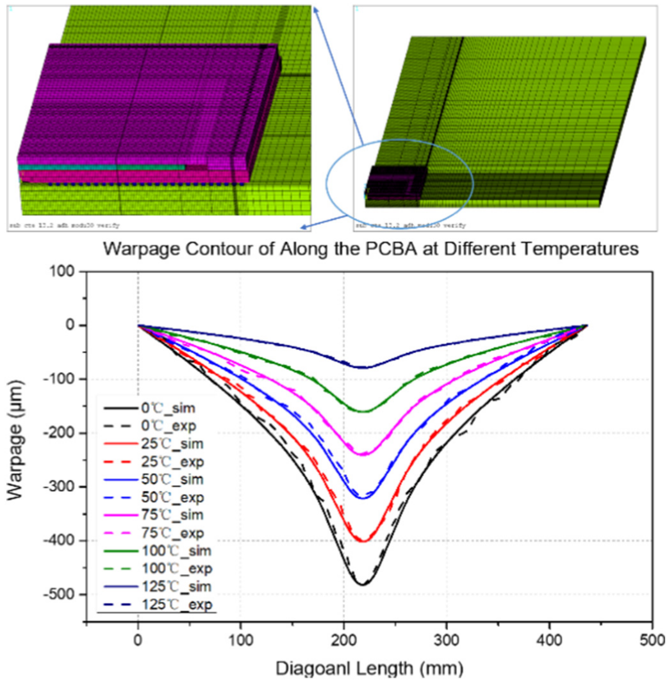

Fig. 9. The warpage of the PCBA along its diagonal originated by 3-D DIC and simulation at elevated temperatures.

warpage plot precipitous in the middle area. With a length of more than 400 mm, we plotted the diagonal warpage of a 36″ × 28″ PCB assembly. Currently, the diversity of the electronic products demands different field of views, from the interconnect to PCB or wafer. The reliability assessment can no longer be limited to certain components. For the direct image acquisition and correlation method the sample can be measured and analyzed, as long as there is successful camera calibration. Regarding the unlimited field of view advantage, 3-D DIC provides more support to all levels of electronic devices.

Apart from the warpage, the full-field in-plane strain can be obtained simultaneously when the 3-D DIC measurements are performed. The in-plane strain can be further processed to be the effective CTE. Fig. 10 shows the different CTEs on the printed circuit board (PCB) in *X* and *Y* direction. To connect multiple components on it, the PCB has different copper densities at different locations, which results in the different effective CTEs. The conventional Thermo-Mechanical Analysis requires to prepare the strip samples within certain size in *X* and *Y* directions and at different copper density zones separately. It takes several or tens of measurement to evaluate the CTE on different areas and directions. For image correlation analysis, as the global PCB images are accumulated once, the strain can be calculated in any direction or on any surface. Even when the surface has multiple plateaus or components, the DIC method exports the deformation. The high efficiency

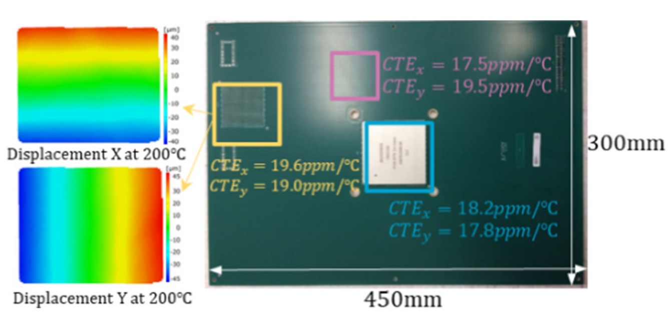

Fig. 10. The different CTE distributions on a PCB with the local displacement contours in *X* and *Y* direction.

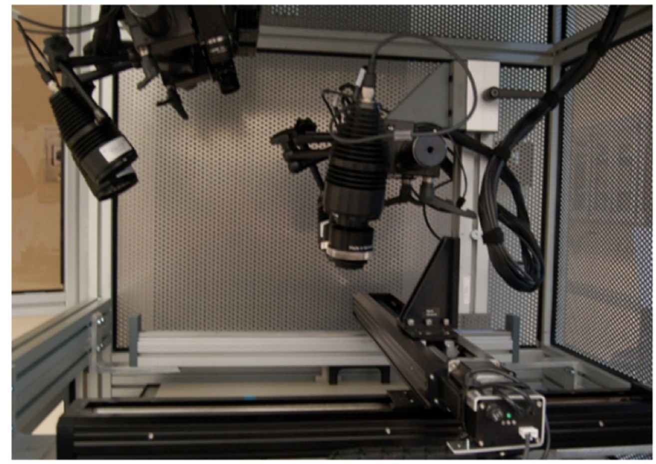

Fig. 11. The experiment setup of dual views 3-D DIC.

CTE assessment from DIC analysis provides the simulation model with more accurate material properties. Moreover, the DIC based CTE results detect the nonuniform expansion that the design team probably wants to avoid, so that the inner stress can be balanced.

During the mass production, the chips are diced from wafer, the substrates are divided from substrate strips, and the molded packages are cut from the whole molded wafer or panel. The quality control of these large parts is significant to the production yield. 3-D DIC has an unlimited field of view, which it uses to perform the warpage measurement of the large product. Some areas can be the high-risk zones, so that the local warpage of each component is also important. Based on these scenarios, the global and local view measurement system was established. Fig. 11 shows the experiment setup of dual views 3-D DIC system. The global sensors are placed on the top of thermal chamber, the same as the conventional 3-D DIC setup in Fig. 8, with light sources to illuminate the entire sample, while the local sensors focus on the detailed areas. The motorized linear stage carries the local sensors to multiple locations at each temperature to capture small view images on many local areas. The measurement accuracy of 3-D DIC is proportional to the field of view because the method is highly dependent on the length of each pixel. Global sensors describe the overall warpage distribution and the local sensors quantify the critical deflection with high sensitivity (Table 1).

The warpage measurement of a 300 mm wafer was performed with the dual views 3-D DIC system (Fig. 12). The global sensors depicted the undulant surface of the wafer at 25 °C and 125 °C. It is notable that the actual wafer cannot be deflected symmetrically. Simulation results are always quarterly symmetrical, but the actual manufacturing process involves diverse stress, chemical shrinkage, and nonuniform heat. The warpage contours showed that temperature loading enhanced the deflection at the wafer center. The initial warpage on the left of the wafer gradually shifted to the center. When the local cameras produced the individual chip warpage at the maximum deflection area, the individual chip did not distort intensively. Its warpage changed from yellow (about 30 μm) to red (45 μm), but it maintains the same surface topography. Though the global sensors predicted the potential risk in the large warpage zone, the local sensors proved that the chip is extruded

Table 1
The parameters of the dual views 3-D DIC system.

Sensor	Focal lens (mm)	Field of view (mm^2)	Accuracy (μm)	Application
Global	17	500 × 400	± 12.5	PCB, wafer, panel
Local	75	20 × 16	± 0.5	Substrate, package, chip

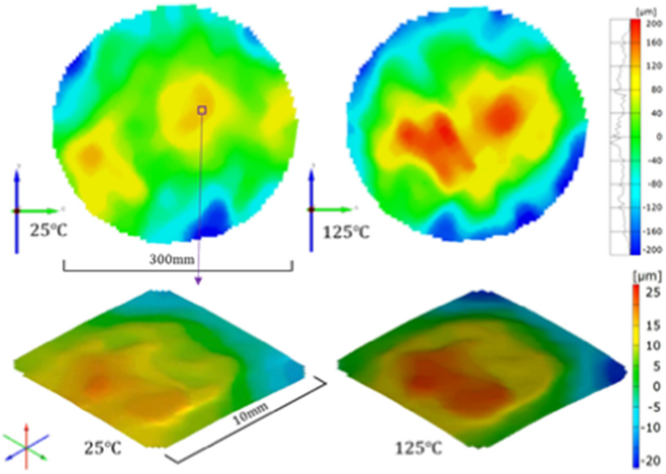

Fig. 12. The warpage contours of a 300 mm wafer and a 10 mm chip on the wafer from dual views 3-D DIC system.

rigidly, which means it moved toward the camera as the rigid motion. The global deformation exacerbates 15 μm chip warpage. Sometimes, the deflection exceeds the standard amount, but it exerts no influence on the yield rate. When the global sensors search for the potential risk, the local sensors can determine it. This system generates the global warpage and local details efficiently, which assists us in understanding some practical issue that requires interpretation with the consideration of both results.

As mentioned before, the diversity of current electronic packages complicates the test condition. For the stacked chips package, the height of the molded package can be 6 mm. The protruding component is connected to the substrate or PCB. To understand the interconnect reliability between package and substrate, the relative warpage variance from top surface to bottom substrate could be an effective way. After the measurement, one data point is selected on the package, and the other point can be defined on the bottom surface. The relative height variance between the two points indicates the deformation of the interconnects. The 6 mm height package generates the blind area on the optical path of the cameras (Fig. 13). The gap of the blind area is close to the interconnects, which is the critical area to understand the relative movement between the package and the substrate. If the bottom surface point is far away from the interconnect, the relative height change loses the confidence to represent the interconnect deformation.

Facing the issue of the blind area gap, the conventional 3-D DIC should be improved. The 3-D profile tool, like the digital volume correlation, utilizes an X-ray to scan the sample [30, 31]. The test specimen

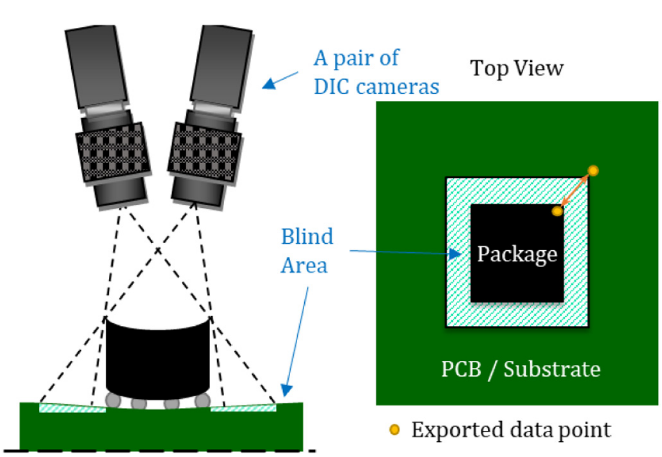

Fig. 13. The schematic of the blind area obstacles for conventional 3-D DIC method.

is spun, while the X-ray continuously scans. Whereas it is difficult to perform the sample spinning during the transient thermal test, the rotation mechanism must be heated together. Instead of spinning the specimen, this work chooses to "rotate the cameras." In other words, two pairs of sensors are placed on the top of the specimen, as if another pair of sensors was duplicated from the other direction. It can be assumed as moving a pair of sensors symmetrically. The schematic in Fig. 14 explains the adjusted stereoscopic DIC system. By modifying the dual views DIC system, four cameras focus on two sides of the sample to guarantee that each pair covers half of the blind area. The sensors on the left and right proceed to perform the image correlation individually, which means they are going to export the contours with less blind area on two sides and more blind areas on the other two sides. After the independent correlation, DIC system will reverse all the coordinate information to the shared world coordinate system. When the first and second pair of the cameras are ensured to be systematical about the *YZ* plane, the rotation matrix Eq. (7) of the second pair 3-D DIC system should be modified as follows:

$$[R'] = \begin{bmatrix} \cos\alpha\cos\gamma & -\sin\alpha\cos\gamma & -\sin\gamma \\ \sin\alpha\cos(\beta-\beta_1-\beta_2) - \cos\alpha\sin(\beta-\beta_1-\beta_2)\sin\gamma & \cos\alpha\cos(\beta-\beta_1-\beta_2) + \sin\alpha\sin(\beta-\beta_1-\beta_2)\sin\gamma & -\sin(\beta-\beta_1-\beta_2)\cos\gamma \\ \sin\alpha\sin(\beta-\beta_1-\beta_2) + \cos\alpha\cos(\beta-\beta_1-\beta_2)\sin\gamma & \cos\alpha\sin(\beta-\beta_1-\beta_2) - \sin\alpha\cos(\beta-\beta_1-\beta_2)\sin\gamma & -\cos(\beta-\beta_1-\beta_2)\cos\gamma \end{bmatrix} \quad (8)$$

where the original γ in Eq. (7) was replaced with $\pi - \gamma$ and β should rotate $\beta_1 + \beta_2$ more in the new 3 × 3 matrix Eq. (8).

The stereoscopic DIC system covers all the blind areas that traditional 3-D DIC system cannot measure. In Fig. 15, the conventional 3-D DIC missed some areas due to the height of tall package, which generates a blind area gap up to 2.5 mm around the packages. With the help of another pair of sensors, the blind area is eliminated, and the missing gap is smaller than 0.6 mm. In this case, the relative height change for the 0.6 mm gap can be referred to by way of understanding the deflects that were generated on the interconnect. One point is selected on the top surface of the package, 0.3 mm away from the upper surface corner, and the other point is on the bottom surface, which is 0.3 mm away to interconnect. The relative height change with the thermal loading is plotted in Fig. 16. Three curves are generated with different gap distances and test systems. It explicitly states that the relative height increases as the temperature enhances. The total difference of the out-of-plane deformation is about 30 μm when the selected two points are 0.6 mm from each other. Meanwhile, the 3-D DIC generates the result with the red dots, which has 2.5 mm gap. The curve barely displays a raising trend, but the deflection amount is less than 15 μm, half of the stereoscopic DIC system. It is evident that the shorter the gap distance is, the more realistic and reliable data it will be. To make sure the coordinate rotation is correct, the same points with 2.5 mm distance are extracted from the stereoscopic DIC system and plotted with blue triangles, which shows the similar trend and values with conventional 3-D DIC.

It can be assumed that if 25 μm is the maximum height tolerance standard for the interconnects, the 15 μm height changes from 2.5 mm gap shows the interconnect is safe; however, the 30 μm variance from the 0.6 mm gap reports the potential risks. The result with a large gap would lead the report in a wrong direction. The objective is to develop the stereoscopic DIC system, which realizes the test ability for the stereoscopic samples. It compensates for the deficiency, which makes digital volume correlation difficult to apply to electronic packaging measurement, e.g., the scanning time delay and the sample rotation. The multiple sensors DIC system can be a good choice to handle the

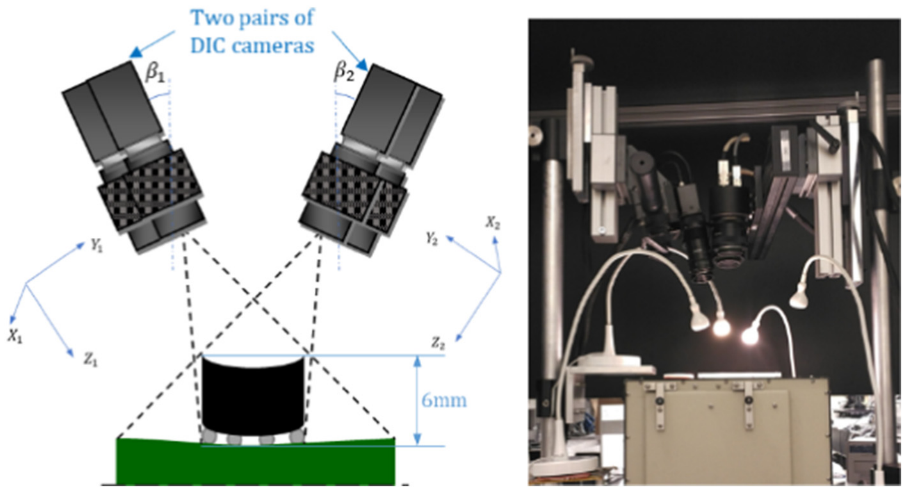

Fig. 14. The schematic and experimental setup of stereoscopic DIC system.

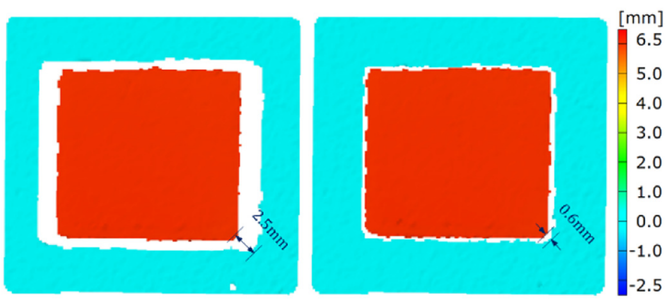

Fig. 15. The warpage contours of the 6 mm tall PCB assembled by 3-D DIC and stereoscopic DIC system.

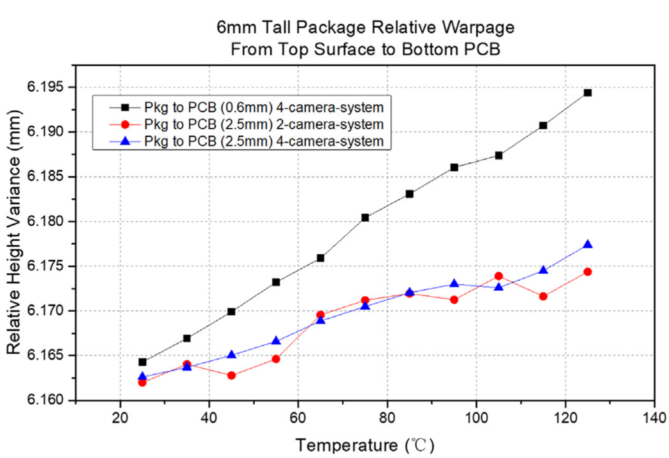

Fig. 16. The height variances from the package top to the bottom substrate when the gap distances are 0.6 mm and 2.5 mm.

complex surface condition measurement request for electronic packages soon.

6. Discussion on advanced 3-D DIC test methods

Regular cameras are capable of capturing 10 to 100 images every second with the shutter time ranging from 100 ms to 10 ms. The frequency is sufficient to learn the deformation during reflow for electronic packages. In addition to thermal load, mechanical shock, such as the drop impact, can also lead to the failure of electronic package. The high-speed DIC system was developed to capture the transient deformation. Instead of the conventional CCD or CMOS cameras, DIC system employs two high-speed cameras that take 10,000 to 100,000 images every second. Fig. 17 shows the experimental schematic of the drop impact test setup with high-speed DIC. Two high-speed cameras focus on the impact surface with halogen light sources that guarantee to illuminate the sample surface in a small aperture.

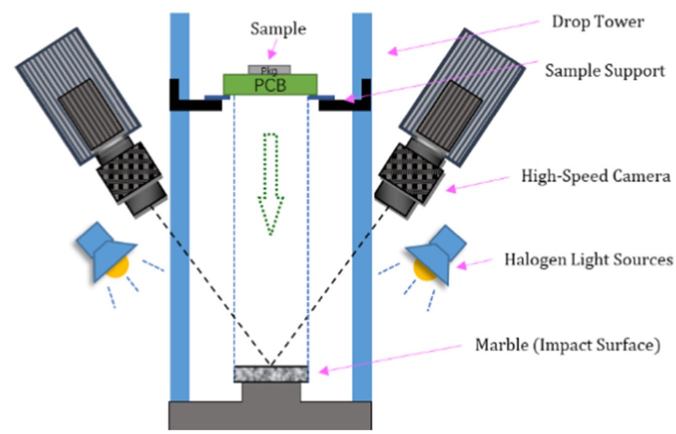

Fig. 17. The schematic of the high-speed DIC experiment setup for drop impact study.

A PCB assembly drop test is shown in Fig. 18 (a)&(b). The symmetric out-of-plane deformation indicates the sample contacts the full surface. If the sample orientation is not well prepared, the contours cannot display a symmetric deformation. The plot provides the first nature frequency around 190 ms to validate the simulation model. The maximum out-of-plane displacement is between −0.45 mm (away from the camera) and 0.2 mm (toward the camera). It can be a strong reference to evaluate the critical components reliability at different drop energies. In the meantime, the numerical model with solidified nature frequency and out-of-plane deformation will instill researchers with enough confidence to predict risks.

7. Summary

With DIC system, the single camera quantifies the local strain, such as the interconnect. Some examples demonstrate the effectiveness of this method in learning the strain concentration. The 2-D DIC with high magnification lens can predict the potential risks before the failure occurs. 3-D DIC interprets the warpage and the in-plane information together.

Due to diverse experiment demands, dual views and stereoscopic DIC are developed. Through the dual views, DIC learns the global and

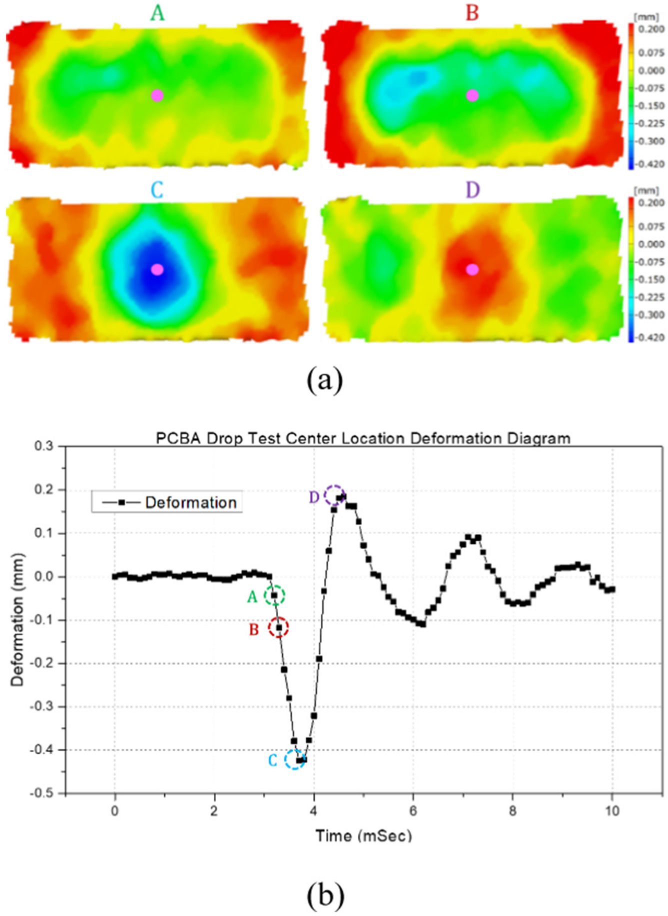

Fig. 18. (a) The out-of-plane deformation of the PCB assembly during drop test; (b) The out-of-plane deformation vs. time plot of the pink point in the center. (For interpretation of the references to colour in this figure legend, the reader is referred to the web version of this article.)

local warpage simultaneously, which appears to be the coarse global model and fine local model in simulation. The overall warpage and the local details assist to evaluate the reliability and recognize the high-risk zone. The stereoscopic DIC covers multiple plateaus with four sensors, which can be further developed with more sensors, as long as, the shared coordinates are convertible to the world coordinate. The high-speed DIC displays the deformation with mechanical shock.

This work aims to introduce DIC technique to the electronic packaging realm to fully comprehend and utilize it for failure risk prediction or model verification. The coming decade will be the imaging decade and it will be of great advantage and efficiency to perform the reliability assessment of electronic packages with fully developed DIC technique.

References

[1] S. Lee, R. Ramadoss, M. Buck, V.M. Bright, K.C. Gupta, Y.C. Lee, Reliability testing of flexible printed circuit-based RF MEMS capacitive switches, Microelectron. Reliab. 44 (2004) 245–250, http://dx.doi.org/10.1016/j.microrel.2003.09.002.

[2] Y. Guo, Applications of shadow Moiré method in determinations of thermal deformations in electronic packaging, Proc. SEM Spring Conf. Exp. Mech. 1995, pp. 702–708.

[3] Y. Zhao, C. Basaran, A. Cartwright, T. Dishongh, Thermomechanical behavior of micron scale solder joints under dynamic loads, Mech. Mater. 32 (2000) 161–173, http://dx.doi.org/10.1016/S0167-6636(99)00053-8.

[4] B. Han, Y. Guo, H.C. Choi, Out-of-plane displacement measurement of printed circuit board by shadow moiré with variable sensitivity, Proc. 1993 ASME Int. Electron. Packag. Conf., ASME, 1993, pp. 179–185.

[5] T.Y. Tee, Z. Zhong, Integrated vapor pressure, hygroswelling, and thermo-mechanical stress modeling of QFN package during reflow with interfacial fracture mechanics analysis, Microelectron. Reliab. 44 (2004) 105–114, http://dx.doi.org/10.1016/j.microrel.2003.07.004.

[6] A.F. Bastawros, A.S. Voloshin, Transient thermal strain measurements in electronic packages, IEEE Trans. Components, Hybrids, Manuf. Technol. 13 (1990) 961–966.

[7] S. Park, R. Dhakal, R. Joshi, Comparative analysis of BGA deformations and strains using digital image correlation and Moiré interferometry, Proc. Soc. Exp. Mech., Portland, 2005, pp. 1–8.

[8] H.W. Schreier, Advances in light microscope stereo vision, Exp. Mech. 44 (2004) 278–288, http://dx.doi.org/10.1177/0014485104041546.

[9] Y. Niu, H. Lee, S. Park, A new in-situ warpage measurement of a wafer with speckle-free digital image correlation (DIC) method, Proc. 2015 IEEE 65th Electron. Components Technol. Conf. 2015, pp. 425–431, , http://dx.doi.org/10.1109/ECTC.2015.7159627.

[10] M. Sutton, C. Mingqi, W. Peters, Y. Chao, S. Mcneill, Application of an optimized digital correlation method to planar deformation analysis, Image Vis. Comput. 4 (1986) 143–150, http://dx.doi.org/10.1016/0262-8856(86)90057-0.

[11] M. Sutton, W.J. Wolters, W. Peters, W.F. Ranson, S.R. Mcneill, Determination of displacements using an improved digital correlation method, Image Vis. Comput. 1 (1983) 133–139, http://dx.doi.org/10.1016/0262-8856(83)90064-1.

[12] Y. Niu, S. Shao, S.B. Park, C.L. Kao, A novel speckle-free digital image correlation method for in-situ warpage characterization, IEEE Trans. Components, Packag. Manuf. Technol. 7 (2017) 276–284, http://dx.doi.org/10.1109/TCPMT.2016.2635581.

[13] M.A. Sutton, J.J. Orteu, H.W. Schreier, Image Correlation for Shape, Motion and Deformation Measurements: Basic Concepts, Theory and Applications, Springer, New York, 2009, http://dx.doi.org/10.1017/CBO9781107415324.004.

[14] H. Wang, Y. Kang, Improved digital speckle correlation method and its application in fracture analysis of metallic foil, Opt. Eng. 41 (2002) 2793–2798, http://dx.doi.org/10.1117/1.1511749.

[15] J.D. Helm, S.R. Mcneill, M.A. Sutton, Improved three-dimensional image correlation for surface displacement measurement, Soc. Photo-Optical Instrum. Eng. 35 (1996) 1911–1920, http://dx.doi.org/10.1117/1.600624.

[16] Y. Niu, H. Wang, S. Shao, S.B. Park, In-situ warpage characterization of BGA packages with solder balls attached during reflow with 3D digital image correlation (DIC), Proc. 2016 IEEE 66th Electron. Components Technol. Conf, 2016, pp. 782–788, , http://dx.doi.org/10.1109/ECTC.2016.311.

[17] S. Park, A. Al-Yafawi, D. Yu, J.B. Kwak, J. Lee, N.S. Goo, Influence of fastening methods on the dynamic response and reliability assessment of PCBS in cellular phones under free drop, 2008 11th IEEE Intersoc, Conf. Therm. Thermomechanical Phenom. Electron. Syst. (2008) 876–882, http://dx.doi.org/10.1109/ITHERM.2008.4544358.

[18] O. De Almeida, F. Lagattu, J. Brillaud, Analysis by a 3D DIC technique of volumetric deformation gradients: application to polypropylene/EPR/talc composites, Compos. Part A Appl. Sci. Manuf. 39 (2008) 1210–1217, http://dx.doi.org/10.1016/j.compositesa.2007.08.028.

[19] J.E.D.E.C. Standard, Package Warpage Measurement of Surface-mount Integrated Circuits at Elevated Temperature, JESD22-B112, (2009).

[20] J.B. Kwak, S.B. Park, Integrated hygro-swelling and thermo-mechanical behavior of mold compound for MEMS package during reflow after moisture preconditioning, Microelectron. Int. 32 (2015) 8–17, http://dx.doi.org/10.1108/MI-04-2014-0014.

[21] Y. Niu, H. Wang, S.B. Park, A general strategy of in-situ warpage characterization for solder attached packages with digital image correlation method, Opt. Lasers Eng. 93 (2017) 9–18, http://dx.doi.org/10.1016/j.optlaseng.2017.01.008.

[22] H. Lee, S. Park, Creep strain measurement of an actual leadfree solder interconnect using digital image correlation, ASME 2012 Int. Mech. Eng. Congr. Expo., Houston, 2012, pp. 1–6, , http://dx.doi.org/10.1115/IMECE2012-89799.

[23] T.T. Nguyen, D. Yu, S.B. Park, Characterizing the mechanical properties of actual SAC105, SAC305, and SAC405 solder joints by digital image correlation, J. Electron. Mater. 40 (2011) 1409–1415, http://dx.doi.org/10.1007/s11664-011-1534-z.

[24] S. Guo, M.A. Sutton, N. Li, X.D. Li, L.W. Wang, S. Rajan, Measurement of local thermal deformations in heterogeneous microstructures via SEM imaging with digital image correlation, Exp. Mech. 57 (2017) 41–56, http://dx.doi.org/10.1007/s11340-016-0206-6.

[25] V. Lin, N. Kao, D.S. Jiang, C.S. Hsiao, Stress simulation and design optimal study for Cu pillar bump structure, Proc. 2013 IEEE 15th Electron. Packag. Technol. Conf, 2013, pp. 598–601, , http://dx.doi.org/10.1109/EPTC.2013.6745790.

[26] L. Xue, Y. Niu, H. Lee, D. Yu, S. Chaparala, S. Park, An experimental and numerical study of the dynamic fracture of glass, ASME 2013 Int. Tech. Conf. Exhib., Burlingame, 2013, http://dx.doi.org/10.1115/IPACK2013-73292.

[27] D. Yu, J.B. Kwak, S. Park, J. Lee, Dynamic responses of PCB under product-level free drop impact, Microelectron. Reliab. 50 (2010) 1028–1038, http://dx.doi.org/10.1016/j.microrel.2010.03.003.

[28] M.A. Sutton, S.R. Mcneill, J.D. Helm, Y.J. Chao, Advances in Two-dimensional and three-dimensional computer vision, Photomechanics, Springer, Berlin, 2000, pp. 323–372, , http://dx.doi.org/10.1007/3-540-48800-6_10.

[29] Y. Niu, J. Wang, S.B. Park, The complete packaging reliability studies through one digital image correlation system, Proc. 2017 IEEE 67th Electron. Components Technol. Conf. 2017, pp. 1916–1921, , http://dx.doi.org/10.1109/ECTC.2017.58.

[30] B.K. Bay, T.S. Smith, D.P. Fyhrie, M. Saad, Digital volume correlation: three-dimensional strain mapping using X-ray tomography, Exp. Mech. 39 (1999) 217–226, http://dx.doi.org/10.1007/BF02323555.

[31] C. Franck, S. Hong, S.A. Maskarinec, D.A. Tirrell, G. Ravichandran, Three-dimensional full-field measurements of large deformations in soft materials using confocal microscopy and digital volume correlation, Exp. Mech. 47 (2007) 427–438, http://dx.doi.org/10.1007/s11340-007-9037-9.